ORNL/TM-2022/2689

Development of Laser-Induced Breakdown Spectroscopy for the Californium-252 Supply Program

Sawyer B. Irvine
Hunter B. Andrews
Kristian G. Myhre
Jamie B. Coble

September 2022

OAK RIDGE National Laboratory

ORNL IS MANAGED BY UT-BATTELLE LLC FOR THE US DEPARTMENT OF ENERGY

ORNL/TM-2022/2689

Radioisotope Science and Technology Division

DEVELOPMENT OF LASER-INDUCED BREAKDOWN SPECTROSCOPY FOR THE CALIFORNIUM PRODUCTION PROGRAM

Sawyer B. Irvine,
Hunter B. Andrews
Kristian G. Myhre
Jamie B. Coble

September 2022

Prepared by
OAK RIDGE NATIONAL LABORATORY
Oak Ridge, TN 37831
managed by
UT-BATTELLE LLC
for the
US DEPARTMENT OF ENERGY
under contract DE-AC05-00OR22725

CONTENTS

FIGURES

ACRONYMS

CF-LIBS	calibration-free–laser-induced breakdown spectroscopy
FO-LIBS	fiber-optic laser-induced breakdown spectroscopy
FWHM	full width half maximum
LIBS	laser-induced breakdown spectroscopy
NA	numerical aperture
ORNL	Oak Ridge National Laboratory

EXECUTIVE SUMMARY

Calibration-free–laser-induced breakdown spectroscopy (CF-LIBS) is suggested as an alternative to traditional LIBS because it does not rely on calibration curves and instead relies on previously reported parameters called transition probabilities. Transition probabilities are fundamental parameters that describe the probability a specific transition from an upper energy to a lower energy will occur. These values act as internal calibrations and allow concentrations to be calculated based on the plasma temperature and electron density, which can be determined from Saha-Boltzmann methods. CF-LIBS provides the ability to perform elemental concentration estimations on samples without the need for chemical dilutions and only nanograms of material are ablated into the plasma. These benefits can be applied remotely inside hot cells, glove boxes, and radiation hoods through optical fibers. This report summarizes recent efforts to develop CF-LIBS methods for future applications within Oak Ridge National Laboratory's radioisotope production portfolio, such as the Cf-252 Supply Program. Summaries are provided for the developed Python scripts for data analysis and two studies employing these programs to determine unreported transition probabilities of relevant lanthanides. Additionally, a review of fiber-delivered LIBS and a discussion of a LIBS fiber probe design are provided.

1. BRIEF BACKGROUND

Oak Ridge National Laboratory (ORNL) is one of the nation's largest producers of radioisotopes, with applications ranging from medical treatments to nuclear batteries. One of these production programs is the Cf-252 Supply Program which is one of two producers of Cf-252 in the world. These production programs typically rely on analytical measurements of grab samples that can involve large dilutions and cause delays. This creates a desire for in situ, near-real-time measurements. Optical spectroscopy is well-suited to fit this need; this family of techniques is inherently rapid and can be performed remotely using fiber-optics. Laser-induced breakdown spectroscopy (LIBS) is useful for elemental analysis of solids, liquids, and gasses and can be employed remotely through optic fibers.[1–3] A laser is launched through an optic fiber and then focused from the exiting face of the fiber onto a sample surface so that the material ablates into a plasma and releases optical light characteristic of the sample's elemental constituents. The emitted light can be collected by an optic fiber and transmitted to a spectrometer for analysis. This would allow samples to be analyzed without exposing equipment or personnel to radioactive material.

LIBS typically relies on matrix-matched standards to calculate a sample's concentrations. This is achieved by making standards similar in matrix to your sample and then performing LIBS analysis on each standard, measuring the intensity of a species peak, and then creating a calibration curve of the measured intensities from your standards. Once the calibration curve is made, the unknown sample can be shot with the laser and the emissions analyzed to compare the peak of interest's intensity to the calibration curve to estimate its concentration. The issue with this method is that making matrix-matched standards requires material, and when working with resource-restricted material such as actinides or other radioisotopes, this becomes an unreasonable approach. Calibration-free–LIBS (CF-LIBS) provides an unique alternative for analyzing resource-restricted materials. CF-LIBS relies on previously reported fundamental parameters called transition probabilities to forgo the matrix-matched standard calibration method. The transition probabilities essentially act as internal calibrations and describe the rate at which specific transitions are estimated to occur for a certain species. CF-LIBS can be used to analyze spectra and calculate individual species' concentrations.

Transition probabilities are in short supply for certain elements, especially lanthanides and actinides. As mentioned previously, transition probabilities are required for CF-LIBS, and thus the ability to produce these values is necessary. Methods exist to estimate these values; however, they typically require an amount of material that is difficult to obtain for the actinides. A less resource-intensive method would allow for

transition probabilities to be estimated for the rare analytes relevant to radioisotope production. Our team has proposed using LIBS measurements themselves to estimate transition probabilities, taking advantage of the LIBS trait of very low material consumption (i.e., ~nanograms per shot).

This report details Python programs developed under this project to facilitate the analysis and processing of large spectral datasets. These programs were used during the two summarized studies in which LIBS has been used to estimate transition probabilities for lanthanides (except for promethium). Lastly, a future-looking review and discussion of fiber-optic LIBS is provided.

2. PYTHON PROGRAMS FOR LASER-INDUCED BREAKDOWN SPECTROSCOPY ANALYSIS

Python was used to write the scripts used for data analysis/processing. It was also used to begin work on a peak identifier executable software. The scripts used were separated into sections and will be described below in order of application.

2.1 EFFICIENCY CORRECTION

The efficiency of the optical system needed to be accounted for prior to any data analysis. The system includes anything in the optical pathway from the plasma to the detector including focusing optics, fiber-optics, and the spectrometer itself. This was investigated by taking the measured spectrum of a calibration lamp (StellarNet, SL1-CAL) and comparing it against the certified spectrum. This process followed the steps below.

1. Input file paths for the files containing the measured calibration source, the ideal curve for the calibrated source, and the experimental data are given to the program.
2. Each of those are read into the program.
3. Files are formatted into data frames.
4. An interpolation function was used to match the wavelength resolution of the measured and certified spectra.
5. The measured and certified spectra were normalized.
6. The efficiency curve was calculated as the smoothed measured calibration divided by the normalized ideal curve.
7. The experimental data to be used for transition probability estimations was then divided by the calculated efficiency curve.
8. The efficiency-corrected experimental data was exported to a new folder.

2.2 AVERAGING SPECTRA AND BACKGROUND CORRECTION

The collected spectra for the sample was averaged together in groups of 15. Each sample was shot 45 times, producing 3 averaged spectra per sample. The averaged spectra were normalized and background-corrected. For the later study, an Al peak was chosen for normalizing all the data. This process followed the steps below.

1. File paths for the experimental spectra were given to the program, and the files were read into data frames.
2. The data frames were set up such that the wavelength of the spectra were the index values (i.e., row labels) and the columns were the spectra intensity values.
3. Every 15 columns, or spectra, were averaged.
4. Each averaged spectrum was normalized to an Al peak by dividing the entire spectrum by the Al peak intensity.

5. Background correction was applied to each spectrum.
    a. The spectra were stepped through in 1 nm increments, and the local minima was recorded for each section.
    b. A polynomial function was fit to the list of minima found using a Savitsky-Golay filter to create a pseudo-baseline.
    c. The pseudo-baseline was subtracted from the spectrum to remove the background contribution to the signal intensities.

The averaged and corrected spectra were exported to a new file.

2.3 PEAK FITTING

The peaks of interest were fit with Voigt functions to approximate the integral intensity for future calculations. A Voigt function is a combination of Gaussian and Lorentzian functions that have been reported to fit LIBS signals well.[4,5] The Voigt function fits the steepness of the peak sides well and models the tails of the peaks while also providing a general Gaussian curve. This process followed the steps below.

1. The averaged and corrected spectra from the previous section were loaded into the program.
2. A file containing the peak start and stop locations was loaded into the program. The start and stop locations specified where the beginning of a spectral peak was and where the end of it was, determined by the user.
3. The starts, stops, and spectra were input to a function that went through the spectra to fit peaks with Voigt functions.
    a. The program was provided a start, stop, and spectra.
    b. Temporary spectra were trimmed to contain only the start, stop, and points in between.
    c. A Voigt function was fit to the trimmed spectra using the lmfit toolkit.
    d. The function returned the center, area, and full width half maximum (FWHM) for each fitted peak. (Note six spectra per sample resulted from this step because there were three averaged spectra per sample and the samples were made in duplicates).
    e. This process was iterated through the list of peak starts and stops.
4. For each sample, the average and standard deviation of each peak area and FWHM were taken and recorded in a data frame.

All of this information was exported to a new folder, with each sample having its own individual file (i.e., peak area averages and standard deviations). FWHM values were recorded only for the 656 nm hydrogen peak and was exported as an additional file.

2.4 MATCHING PEAK INFORMATION

This section of program collected the information needed to create Saha-Boltzmann plots from a database and append it to the list of the peaks designated from the data. The database was made beforehand from data in the National Institute of Standards and Technology Atomic Spectra Database. The information needed was ionization level, lower and upper energy levels, lower and upper energy-level degeneracies, reported transition probabilities, and emission wavelengths. The program is described below.

1. The database containing all reported information for all elements, neutral and singly ionized, was loaded.
2. A list of the fitted peaks from the previous section, the database, and a True or False statement is fed to a function.
    a. The True or False statement dictates whether the database will be restricted to certain elements during the search procedure.

        i. If the value is True, the user will input elemental abbreviations, and then when finished, the database will be filtered to retain only information for the elements entered.
    b. Once the database is ready, the function uses the list of peaks, which already has energy data calculated from reported energy levels, to match the upper and lower energy levels to ones in the existing database with a tolerance of 0.0001 eV.
    c. When a match is found, the relevant information will be collected into a list that is appended to the initial wavelength list fed to the function once all matches have been found.
3. Next, a new data frame containing information for all matched wavelengths is returned to the user.
4. The columns are named and filtered in order of the reported transition probabilities so that the peaks without reported transition probabilities are at the end.

The resultant data frame is exported to the folder.

2.5 SAHA-BOLTZMANN PLOTS AND SELF ABSORPTION CORRECTION

This section made the Saha-Boltzmann plots using the data frame from the previous section and then used it to estimate new transition probabilities. Performing the calculations for the new transition probabilities was straightforward; therefore, this discussion will focus on the construction of the Saha-Boltzmann plots and self-absorption correction procedure.

1. The list of information including wavelength, energy levels, degeneracies, transition probabilities, and ionization energies was imported.
2. The list was separated into peaks that have previously reported transition probabilities and peaks that have not.
3. The reported data was used to develop Saha-Boltzmann plots that estimate a temperature and electron density for the plasma using a iterative fitting procedure.
4. After initial values for temperature and electron density were calculated, the self-absorption correction started.
5. The ionized and neutral reported points were ranked in ascending order for energy and descending order for transition probabilities.
6. The reference peaks were chosen based on the combined highest numerical rank (i.e., a peak with high energy level and a low transition probability is the best reference peak candidate).
7. The nonreference intensities were divided by the reference intensities, and a correction factor was determined.
8. That correction factor was multiplied by the nonreference intensities to correct them.
    a. If the correction factor was greater than one, it was set to one so that those intensities were not affected.
9. The Saha-Boltzmann plot was made from these corrected and reference peaks.
10. The Saha-Boltzmann plot was fit with a linear regression.
11. The process was repeated until consecutive coefficients of determination (R^2) were below a defined percent difference.
12. Once this iterative process was completed, the new transition probabilities were calculated along with their uncertainties.
13. In addition to these steps, the transition probabilities from the different samples were combined for a Gaussian averaged value and uncertainty. The final calculated transition probabilities were then exported.

3. SUMMARY OF TRANSITION PROBABILITY ESTIMATION STUDIES

3.1 EUROPIUM TRANSITION PROBABILITY ESTIMATION

The samples used in the Eu study consisted of europium oxide (99.95%, Alfa Aesar) mixed with high-purity graphite powder (99.9995%, metal basis, Alfa Aesar), and were pressed into pellets with ~15 ton cm^{-2}. The 1 cm diameter and nominally 2 mm thick pellets were held under pressure for ~2 min after pressure had stabilized. The nominal composition of the first pellet was made to be 1.3, 96.7, and 2.0 atom% of Eu, C, and O, respectively. A second pellet with a different Eu concentration was made to validate calculated transition probabilities. The composition of the second pellet was made to be 1.6, 96.0, and 2.4 atom% of Eu, C, and O, respectively.

All LIBS measurements were performed using (1) an Applied Photonics LIBSCAN-150 laser system with a wavelength of 1,064 nm, an energy per pulse of 161 ± 2.25 mJ, a pulse length of 5 ns, a spot-size diameter of 500 μm, and a laser fluence of 82 J cm^{-2}; (2) a Catalina Scientific Instruments EMU-120/65 echelle spectrometer with a Raptor Falcon Blue electron multiplying charged couple device detector ($\lambda/\Delta\lambda \approx$ 12000); and (3) a Quantum Composers pulse generator. The spectrometer integrations were performed with a gate delay of 1 μs and a gate width of 100 μs. The experimental system used in this study was similar to those previously reported.[6,7] Prior to any measurements, the spectrometer wavelength was calibrated using a StellarNet Inc. SL2 mercury argon lamp, and the spectral efficiency was calculated using a StellarNet Inc. SL1-CAL tungsten halogen lamp with a certified spectrum.

The first pellet made for the Eu study was used to calculate new transition probabilities by using previously reported transition probabilities. The previously reported data was combined with the intensities of matching transitions observed in the spectra to calculate the y-coordinates for a Saha-Boltzmann plot. Saha-Boltzmann plots are used to estimate the temperature and electron densities of the plasma by iteratively fitting the data until the error between iterations reaches a user-defined value (e.g., 0.0001% difference). The temperature and electron density are then used to calculate new transition probabilities.

The second pellet was used to validate the newly estimated transition probabilities. The pellets were shot with the LIBS system described above, and data analysis was performed similarly as described in Section 2. The largest difference between this study and the 13-lanthanide study described in Section 3.2 was that self-absorption correction was not performed in the Eu study. There were also far fewer samples used for the Eu study, which contributed to higher uncertainty in the estimated transition probabilities. The primary purpose of this study was to determine the best way to estimate transition probabilities using LIBS. It was found that Saha-Boltzmann plots, as opposed to Boltzmann plots or single peak calculations, provided the best results. Further information can be found elsewhere. [8,9]

3.2 TRANSITION PROBABILITY ESTIMATION FOR LANTHANIDES

As a follow-up to the Eu study discussed in Section 3.1, similar methods were applied to 13 lanthanide elements to estimate unreported transition probabilities. These were La, Ce, Pr, Nd, Sm, Gd, Tb, Dy, Ho, Er, Tm, Yb, and Lu. An individual sample was made for each lanthanide. Each lanthanide sample was spiked with Sr as an internal standard. Strontium was selected due to its strong spectral response and well-characterized emission peaks with well-known transition probabilities. Each lanthanide and Sr solution was made from Inorganic Ventures 10,000 μg ml-1 inductively coupled plasma standards. Three different concentrations were made for each lanthanide–Sr combination. The three different molar ratios of the lanthanide to Sr were 10, 5, and 2. A 10 μl droplet of each solution was pipetted onto individual aluminum-6061 pucks. The aluminum pucks were machined to have a small recession in the center where the droplet would rest (Figure 1).

Figure 1. The aluminum pucks with a droplet in the center recession (left) and an aluminum puck after being shot with a laser (right).

The pucks were placed onto a hot plate, set to a low temperature, until the solution had completely dried. Duplicate samples were prepared for each concentration. The varied molar ratios, replicate samples, and use of aluminum substrates were adjustments made based on a previously reported study[9] intended to help increase confidence in the transition probabilities determined in this study.

The transition probabilities estimated in this study were calculated using the same methodology as the previous study, with the addition of a self-absorption correction procedure. The results of the study, detailed below, indicated that the following two alterations greatly reduced uncertainty levels.

1. The number of samples taken was greatly increased, which helped reduce uncertainty.
    a. Each sample (10, 5, or 2 molar ratio) was made in duplicate, and each duplicate was shot 45 times. For each element, a total of 270 measurements were taken. This large amount of data improved the statistics for the estimations.
2. Self-absorption correction was employed, which greatly reduced the uncertainty.
    a. The procedure detailed in Section 2 was applied and increased the accuracy of the Saha-Boltzmann fit to the data.[10]

While the uncertainty in the Eu study was as low as 35%, estimations in this study reached as low as 8%. Further details on this study are provided elsewhere.[9]

4. FIBER-DELIVERED LASER-INDUCED BREAKDOWN SPECTROSCOPY REVIEW

A major benefit of LIBS is the ability to utilize fiber-optics for laser delivery and emission collection during analysis.[11–26] This section reviews previous reports of fiber-optic (FO)-LIBS, including configurations, results, and lessons learned. This information will be crucial for establishing an in-house FO-LIBS system.

In Guirado et al.,[12] a submersible LIBS system was designed that launched a Q-switched Nd:YAG 1,064 nm laser through a 45 m, 550 µm core diameter, UV-grade, high-OH fiber. A maximum of 35–40 mJ pulse^{-1} with a pulse width of 7 ns was usable for this configuration. The resulting output energy was 16.5 mJ pulse^{-1}. The same fiber was used to receive the emitted light from the LIBS plasma. The probe head consisted of a pair of lenses: (1) focal length (f) = 38 mm and (2) f = 35 mm. The remote instrument covered a spectral range of 350–550 nm.

Nakanishi et al.[13] launched a Q-switched Nd:YAG 1064 nm and 6 ns laser. It was coupled into a high-OH optical fiber (5 m; 1 mm core diameter; numerical aperture (NA): 0.12; 1,000 ppm OH in the fiber; 4 wt% F in the cladding). The laser was fired through a convex lens (f = 125 mm), and the optic fiber was placed at the focal point or close to it. The beam (10 mJ pulse^{-1}) was focused onto the sample surface with two lenses—f = 40 mm and f = 12.5 mm—equipped on the probe head. The laser spot size was 350 µm in diameter. The same optics were used to collect the emitted light, and a pierced mirror was used to reflect the collected light into an echelle spectrometer. They report that launching the 1,064 nm laser was more resistant to laser attenuation than other (shorter) wavelengths.

Saeki et al.[14] used Q-switched Nd:YAG 1,064 nm lasers with a pulse duration of 6 ns. The laser was reportedly launched at 5–10 mJ using a single lens (f = 125 mm). Both single- and double-pulse configurations were employed. The fiber length was 3–20 m with a core diameter of 0.55–1.0 mm and an NA of 0.12–0.22. The probe head contained an achromatic lens pair, which helped compensate for any chromatic aberration: Lens 1 (f = 32.5 mm and NA = 0.47) and Lens 2 (f = 15.4 mm and NA = 0.58). It was specified that the use of achromatic lenses helped irradiate the laser beam in good condition. They were able to achieve an ablation diameter of 500 µm. It is stressed that the probe head should be designed to collect as much of the diffuse laser beam that exits the optic fiber as possible.

Marquardt et al.[15] used a frequency-doubled Q-switched Nd:YAG laser operated at 532 nm and another laser operating at 1,064 nm. Laser energy at the probe tip was typically 4.2–19 mJ depending on the fiber-optic probe used. The probes were dual fiber. For launching, fiber diameters of 600 and 1,000 µm were used. The fibers were 4 m in length, and all fibers had an NA of 0.48. The laser was launched into the probe via a single lens with a focal length of 8 in (~200 mm). To reduce damage to the fiber tip, a pinhole was placed just in front of the fiber that had a diameter slightly smaller than the fiber. As with the previously detailed studies, there was a pair of additional lenses placed after the probe to collimate and focus the laser onto the sample surface.

In Sasazawa et al.,[16] a Q-switched Nd:YAG laser with a wavelength of 1,064 nm and a pulse width of 7 ns was used. The laser was coupled to a hollow optical fiber with an inner diameter of 700 µm with a focal lens of 250 mm. The focal point of the laser was set at the face of the optic fiber. The emitted light from the laser ablation was transmitted to a spectrometer by pure-silica-glass optical fiber with a core diameter of 400 µm and an NA of 0.22. The reported pulse energies used were 22–16 mJ.

Rai et al.[17] performed FO-LIBS using an Nd:YAG laser operated at 532 nm with a pulse width of 8 ns. A spherical plano-convex fused silica lens with f = 100 mm was used to couple the laser beam into the fiber. The focal point was placed in front of the fiber-optic at 5 mm. The laser energy was 30 mJ. A pinhole cover of 0.8 mm was placed just in front of the fiber to protect it from the ablation. They approximated that ~0.6–0.7 mm of the core was illuminated. The core diameter of the fiber was 1.0 mm and had an NA of 0.16. The same fiber was used for delivery and collection of the light.

Wu et al.[18] used a FO-LIBS setup with three Nd:YAG lasers at 1,064 nm with 10, 15, and 6 ns pulse widths and 40, 60, and 5.5 mJ pulse^{-1}, respectively. The optic fibers were 3, 10, and 75 m long with 800, 1,000, and 550 µm cladding diameters, respectively. The last fiber was an all-silica fiber. It was suggested that

1,000 pm OH-containing optical fiber would have sufficient radiation resistance for radiation-induced transmission losses.

Davies et al.[19] used a Q-switched Nd:YAG laser operated at 1,064 nm and different harmonics. A fused silica fiber with a core diameter of 550 µm was used with laser pulses up to 50 mJ. This fiber was selected as it was sufficiently resistant to "blinding" in an environment of high-dose radiation. The fiber exposed to the radiation showed transmission interference mainly in the UV region; however, it returned to normal functionality once it was removed from the radiation environment. In this study's configuration, two separate fibers were used for laser delivery and emitted light collection, respectively.

Cremers et al.[20] used a Q-switched Nd:YAG laser operated at 1,064 nm. A 5 m fiber was connected to a sampling head that contained the focusing optics for the laser exiting fiber. The fiber was an "anhydroguide G low OH Vis-IR fiber" with 1,500 µm diameter. The input energy to the fiber was reported as 100 mJ with the energy incident on the sample was 84 mJ.

Whitehouse et al.[21] used Q-switched Nd:YAG laser operated at 1,064 nm with a 6 ns pulse width. The laser was launched into a 550 µm core, all-silica optical fiber by a 200 mm focal length lens placed 260 mm in front of the input face of the fiber.

Fobar et al.[22] used a Nd:YAG 1,064 nm laser with a 10 ns pulse width. Reportedly, the 1,064 nm wavelength gave a much higher signal-to-noise ratio for a peak of interest than the 532 nm harmonic. The beam was focused onto a cleaved fiber tip with a 1,000 µm core diameter. The fiber was 25 m long.

Beddows et al.[23] used a single fiber of 20 m with a core diameter of 550 µm and an NA of 0.22. The fiber was prepared with a cleaving process that provided fault-free optical surfaces. The laser used was a Q-switched Nd:YAG laser operated at 1,064 nm and a pulse width was 9 ns. The input energy to the fiber was typically 10–30 mJ. The laser was focused by a single lens with a focal length of 330 mm. The laser was passed through a pierced meter with a 4 mm hole. The energy was not high enough to cause breakdown in air before the fiber.

Fortes and Laserna[24] discuss multiple portable LIBS instruments. Each are reported to be 1,064 nm Nd:YAG lasers. Fiber-optics are 2 m in length, and they are used to analyze soils, paint, particles on filters, steel, organic, hazardous material, speleothems, bronze, cathedral, and road sediments.

Neuhausser et al.[25] used a Nd:YAG laser at 1,064 nm with a pulse width of 10 ns and maximum pulse energy of 200 mJ. It also had the second harmonic at 532 nm, with a pulse width of 8 ns, and energy of 30 mJ. An f = 200 mm lens was used to launch the 1,064 nm laser and f = 80 mm. Plasma breakdown in front of the fiber was avoided but with the increased focal length, more core/cladding breakdown during long-term operation was observed. A total fiber length of 12 m was used.

In Xiao et al.,[26] a Q-switched Nd:YAG laser with pulse width of 10 ns was operated at 1,064 nm. The double pulse was coupled into a 10 m long fiber that had a 1,000 µm core and NA of 0.39. The beam was focused with a plano-convex lens (f = 300 mm). The fiber was placed slightly beyond the 300 mm focal point to catch the divergent light. Two tight-focusing plano-convex lenses (30 mm focal length) were used to collimate and focus the light exiting the fiber onto the sample surface. The emitted light from the plasma was collected by a separate fiber at a 45° angle.

From this information, it is suggested that the laser be focused before the face of the fiber-optic with the fiber optic collecting the divergent light. In this configuration, the divergent light will need to be collimated and refocused at the exit of the optic fiber. Using a fiber with a core diameter of 500 µm or greater is suggested to avoid laser damage. A laser wavelength of 1,064 nm results in fewer reported issues and is

likely the best candidate. It seems it would be beneficial to use a probe head. Many sources use two fibers, one for delivery and one for collection. It is suggested that future work pursue the same method so that collection optics can be separately tuned for the plasma and, if the launching fiber is damaged, so it can be cleaved and refinished without affecting the collection fiber. Purge gas would also benefit both the launching of the laser and the ablation. A purge gas can reduce the chance of ablating at the focal point before the launch fiber and help protect the fiber face.

If two optic fibers are used—one for launching and one for collection—it is suggested that the collection angle be minimal off the launched laser to maintain a compact design. It is desirable for the probe head to be easily manipulated so that it can be optimally positioned for different samples. Typically, a single sample would be shot multiple times. Many shots can be repeated in the same position, but changing locations on the sample helps account for spatial variations in the measurements. Fobar et al.[22] gives a unique design for their probe head. It contains all the optics (i.e., collimating, focusing, and a reflecting mirror) for the launching fiber, and then contains the optics (i.e., mirror, focusing lens) for collection in a separate module angled at 45° from the plasma. A similar design is shown in Figure 2 for a proposed FO-LIBS system with key characteristics such as laser wavelength and core diameter explicitly defined. Initial fiber-launching experiments were performed this year using 1,000 µm fibers and a 1,064 nm laser, with ranging levels of success, but the laser energy transmitted was far from sufficient. Additional efforts will be required to optimize launching configurations.

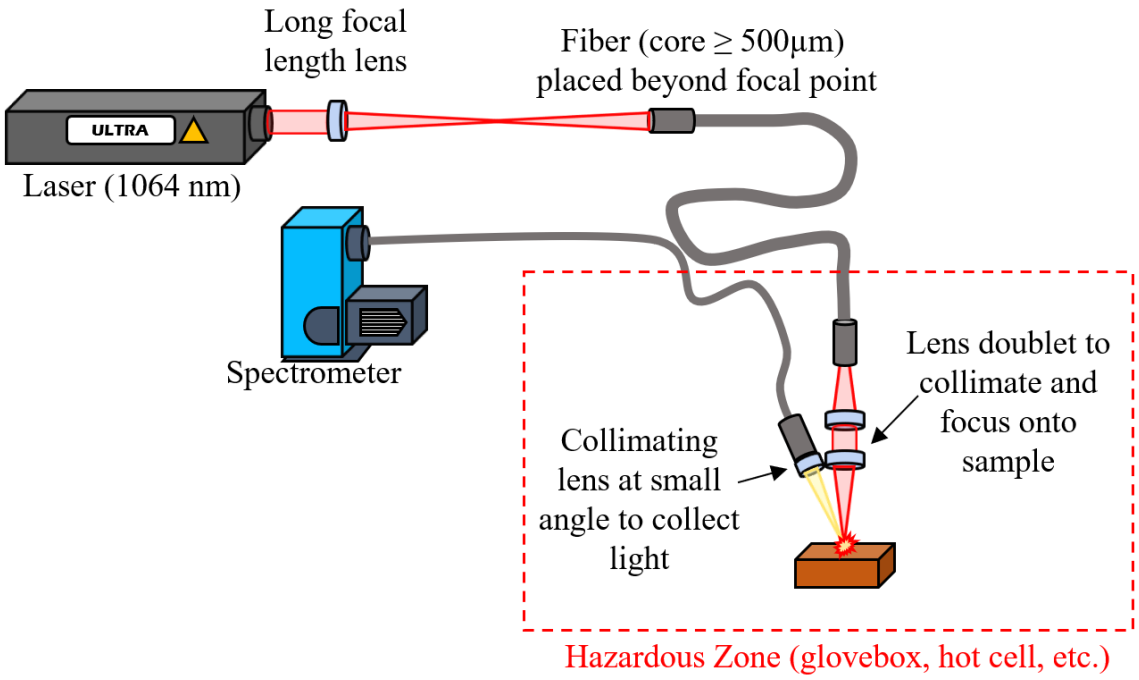

Figure 2. Diagram of proposed FO-LIBS system with key characteristics identified during literature review defined.

5. SUMMARY

This year's efforts toward the development of LIBS for the Cf-252 Supply Program have resulted in significant developments, including the generation of new Python programs for processing and analyzing high-dimensionality spectra, a proven procedure for transition probability estimation, and a comprehensive

review of previous FO-LIBS studies. Future work will involve development of an in-house FO-LIBS system to enable the use of LIBS more readily in process glove boxes and hot cells. This will require significant efforts aimed at optimizing laser-launching configurations to maximize laser energy throughput and minimize degradation of fibers over time. Additionally, a LIBS probe head with integrated optics should be constructed with input from glove box/hot cell support staff and facility safety officers such that it meets functionality and safety requirements for deployment.

6. ACKNOWLEDGMENTS

The authors would like to acknowledge Julie Ezold, John Neal, and Sam Schrell for their assistance. This research was supported by the US Department of Energy Isotope Program, managed by the Office of Science for Isotope R&D and Production. This work used resources at the Radiochemical Engineering Development Center operated by ORNL.

7. REFERENCES

(1) Aguilera, J. A.; Aragón, C. Characterization of a Laser-Induced Plasma by Spatially Resolved Spectroscopy of Neutral Atom and Ion Emissions. *Spectrochim. Acta Part B At. Spectrosc.* **2004**, *59* (12), 1861–1876. https://doi.org/10.1016/j.sab.2004.08.003.

(2) Yang, Y.; Hao, X.; Ren, L. Correction of Self-Absorption Effect in Calibration-Free Laser-Induced Breakdown Spectroscopy(CF-LIBS) by Considering Plasma Temperature and Electron Density. *Optik* **2020**, *208*, 163702. https://doi.org/10.1016/j.ijleo.2019.163702.

(3) Capitelli, M.; Capitelli, F.; Eletskii, A. Non-Equilibrium and Equilibrium Problems in Laser-Induced Plasmas. *Spectrochim. Acta Part B At. Spectrosc.* **2000**, *55* (6), 559–574. https://doi.org/10.1016/S0584-8547(00)00168-3.

(4) de Oliveira Borges, F.; Ospina, J. U.; de Holanda Cavalcanti, G.; Farias, E. E.; Rocha, A. A.; Ferreira, P. I. L. B.; Gomes, G. C.; Mello, A. CF-LIBS Analysis of Frozen Aqueous Solution Samples by Using a Standard Internal Reference and Correcting the Self-Absorption Effect. *J. Anal. At. Spectrom.* **2018**, *33* (4), 629–641. https://doi.org/10.1039/C7JA00299H.

(5) Newville, M.; Stensitzki, T.; Allen, D. B.; Ingargiola, A. LMFIT: Non-Linear Least-Square Minimization and Curve-Fitting for Python, 2014. https://doi.org/10.5281/zenodo.11813.

(6) Sheng, L.; Zhang, T.; Wang, K.; Tang, H.; Li, H. Quantitative Analysis of Fe Content in Iron Ore via External Calibration in Conjunction with Internal Standardization Method Coupled with LIBS. *Chem. Res. Chin. Univ.* **2015**, *31* (1), 107–111. https://doi.org/10.1007/s40242-014-4318-1.

(7) Umar, Z. A.; Liaqat, U.; Ahmed, R.; Hedwig, R.; Ramli, M.; Marpaung, M. A.; Kurniawan, K. H.; Pardede, M.; Baig, M. A. Determination of Micronutrients and Toxic Elements in Moringa Oleifera Leaves by Calibration Free Laser-Induced Breakdown Spectroscopy (LIBS). *Anal. Lett.* **2022**, *55* (5), 755–769. https://doi.org/10.1080/00032719.2021.1966794.

(8) Irvine, S.; Andrews, H.; Myhre, K.; Goldstein, K.; Coble, J. Radiative Transition Probabilities of Neutral and Singly Ionized Europium Estimated by Laser-Induced Breakdown Spectroscopy (LIBS). *J. Quant. Spectrosc. Radiat. Transf.* **2022**, *286*, 108184. https://doi.org/10.1016/j.jqsrt.2022.108184.

(9) Irvine, S. Estimation of Transition Probabilities by Laser-Induced Breakdown Spectroscopy for the Expanded Application of Calibration Free Methods, University of Tennessee - Knoxville, 2022.

(10) Sun, L.; Yu, H. Correction of Self-Absorption Effect in Calibration-Free Laser-Induced Breakdown Spectroscopy by an Internal Reference Method. *Talanta* **2009**, *79* (2), 388–395. https://doi.org/10.1016/j.talanta.2009.03.066.

(11) Griffiths, T. L.; Woodbury, S. E.; Brooks, A.; Pinon, V.; Giakoumaki, A.; Whitehouse, A. I. A Study of the Effects of Gamma Radiation on Optical Components Used in Specially Constructed

Hot Cell Laser-Induced Breakdown Spectroscopy (LIBS) Instruments. *Spectrochim. Acta Part B At. Spectrosc.* **2021**, *180*, 106205. https://doi.org/10.1016/j.sab.2021.106205.
(12) Guirado, S.; Fortes, F. J.; Lazic, V.; Laserna, J. J. Chemical Analysis of Archeological Materials in Submarine Environments Using Laser-Induced Breakdown Spectroscopy. On-Site Trials in the Mediterranean Sea. *Spectrochim. Acta Part B At. Spectrosc.* **2012**, *74–75*, 137–143. https://doi.org/10.1016/j.sab.2012.06.032.
(13) Nakanishi, R.; Saeki, M.; Wakaida, I.; Ohba, H. Detection of Gadolinium in Surrogate Nuclear Fuel Debris Using Fiber-Optic Laser-Induced Breakdown Spectroscopy under Gamma Irradiation. *Appl. Sci.* **2020**, *10* (24), 8985. https://doi.org/10.3390/app10248985.
(14) Saeki, M.; Iwanade, A.; Ito, C.; Wakaida, I.; Thornton, B.; Sakka, T.; Ohba, H. Development of a Fiber-Coupled Laser-Induced Breakdown Spectroscopy Instrument for Analysis of Underwater Debris in a Nuclear Reactor Core. *J. Nucl. Sci. Technol.* **2014**, *51* (7–8), 930–938. https://doi.org/10.1080/00223131.2014.917996.
(15) Marquardt, B. J.; Goode, S. R.; Angel, S. M. In Situ Determination of Lead in Paint by Laser-Induced Breakdown Spectroscopy Using a Fiber-Optic Probe. *Anal. Chem.* **1996**, *68* (6), 977–981. https://doi.org/10.1021/ac950828h.
(16) Sasazawa, S.; Kakino, S.; Matsuura, Y. Optical-Fiber-Based Laser-Induced Breakdown Spectroscopy for Detection of Early Caries. *J. Biomed. Opt.* **2015**, *20* (6), 065002. https://doi.org/10.1117/1.JBO.20.6.065002.
(17) Rai, A. K.; Zhang, H.; Yueh, F. Y.; Singh, J. P.; Weisberg, A. Parametric Study of a Fiber-Optic Laser-Induced Breakdown Spectroscopy Probe for Analysis of Aluminum Alloys. *Spectrochim. Acta Part B At. Spectrosc.* **2001**, *56* (12), 2371–2383. https://doi.org/10.1016/S0584-8547(01)00299-3.
(18) Wu, J.; Qiu, Y.; Li, X.; Yu, H.; Zhang, Z.; Qiu, A. Progress of Laser-Induced Breakdown Spectroscopy in Nuclear Industry Applications. *J. Phys. Appl. Phys.* **2020**, *53* (2), 023001. https://doi.org/10.1088/1361-6463/ab477a.
(19) Davies, C. M.; Telle, H. H.; Montgomery, D. J.; Corbett, R. E. Quantitative Analysis Using Remote Laser-Induced Breakdown Spectroscopy (LIBS). *Spectrochim. Acta Part B At. Spectrosc.* **1995**, *50* (9), 1059–1075. https://doi.org/10.1016/0584-8547(95)01314-5.
(20) Cremers, D. A.; Barefield, J. E.; Koskelo, A. C. Remote Elemental Analysis by Laser-Induced Breakdown Spectroscopy Using a Fiber-Optic Cable. *Appl. Spectrosc.* **1995**, *49* (6), 857–860. https://doi.org/10.1366/0003702953964589.
(21) Whitehouse, A. I.; Young, J.; Botheroyd, I. M.; Lawson, S.; Evans, C. P.; Wright, J. Remote Material Analysis of Nuclear Power Station Steam Generator Tubes by Laser-Induced Breakdown Spectroscopy ☪. *At. Spectrosc.* **2001**, 10.
(22) Fobar, D. G.; Xiao, X.; Burger, M.; Le Berre, S.; Motta, A. T.; Jovanovic, I. Robotic Delivery of Laser-Induced Breakdown Spectroscopy for Sensitive Chlorine Measurement in Dry Cask Storage Systems. *Prog. Nucl. Energy* **2018**, *109*, 188–194. https://doi.org/10.1016/j.pnucene.2018.08.001.
(23) Beddows, D. C. S.; Samek, O.; Liška, M.; Telle, H. H. Single-Pulse Laser-Induced Breakdown Spectroscopy of Samples Submerged in Water Using a Single-Fibre Light Delivery System. *Spectrochim. Acta Part B At. Spectrosc.* **2002**, *57* (9), 1461–1471. https://doi.org/10.1016/S0584-8547(02)00083-6.
(24) Fortes, F. J.; Laserna, J. J. The Development of Fieldable Laser-Induced Breakdown Spectrometer: No Limits on the Horizon. *Spectrochim. Acta Part B At. Spectrosc.* **2010**, *65* (12), 975–990. https://doi.org/10.1016/j.sab.2010.11.009.
(25) Neuhauser, R. E.; Panne, U.; Niessner, R. Utilization of Fiber Optics for Remote Sensing by Laser-Induced Plasma Spectroscopy (LIPS). *Appl. Spectrosc.* **2000**, *54* (6), 923–927. https://doi.org/10.1366/0003702001950337.
(26) Xiao, X.; Le Berre, S.; Fobar, D. G.; Burger, M.; Skrodzki, P. J.; Hartig, K. C.; Motta, A. T.; Jovanovic, I. Measurement of Chlorine Concentration on Steel Surfaces via Fiber-Optic Laser-

Induced Breakdown Spectroscopy in Double-Pulse Configuration. *Spectrochim. Acta Part B At. Spectrosc.* **2018**, *141*, 44–52. https://doi.org/10.1016/j.sab.2018.01.003.